



PCCP

Structural Aspects of the Topological Model of the Hydrogen Bond in Water on Auto Dissociation via Proton Transfer

Journal:	<i>Physical Chemistry Chemical Physics</i>
Manuscript ID	CP-ART-04-2018-002592.R1
Article Type:	Paper
Date Submitted by the Author:	18-May-2018
Complete List of Authors:	Lentz, Jesse; Rutgers University, Materials Sci. and Eng. Garofalini, Stephen; Rutgers University, Materials Sci. and Eng.

SCHOLARONE™
Manuscripts

Structural Aspects of the Topological Model of the Hydrogen Bond in Water on Auto-Dissociation via Proton Transfer

Jesse Lentz and Stephen H. Garofalini

Department of Materials Science and Engineering
Rutgers University

Abstract

Molecular dynamics (MD) simulations were used to investigate the structure and lifetimes of hydrogen bonds and auto dissociation via proton transfer in bulk water using a reactive and dissociative all-atom potential that has previously been shown to match a variety of water properties and proton transfer. Using the topological model, each molecule's donated and accepted hydrogen bonds were labeled relative to the other hydrogen bonds on neighboring waters, providing a description of the effect of these details on the structure, dynamics and autoionization of water molecules. In agreement with prior data, asymmetric bonding at the sub-100 femtosecond timescale is observed, as well as the existence of linear, bifurcated, and dangling hydrogen bonds. The lifetime of the H-bond, 2.1 ps, is consistent with experimental data, with short time librations on the order of femtoseconds. The angular correlation functions, the presence of a second shell water entering the first shell, and OH vibrational stretch frequencies were all consistent with experiment or ab-initio calculations. The simulations show short-lived (femtoseconds) dissociation of a small fraction of water molecules followed by rapid recombination. The role of the other H-bonds to the acceptor and on the donor play an important part in proton transfer between the molecules in auto dissociation and is consistent with the role of a strong electric field caused by local (first and second shell) waters on initiating dissociation. The number of H-bonds to the donor water is 4.3/molecule in the simulations, consistent with previous data regarding the number of hydrogen bonds required to generate this strong local electric field that enhances dissociation. The continuous lifetime autocorrelation function of the H-bond for those molecules that experience dissociation is considerably longer than that for all molecules that show no proton transfer.

Introduction

A significant number of studies have been performed in order to understand and quantify the behavior of protons in bulk water¹⁻³⁴. Although recently challenged^{29-31, 35, 36}, the notion of water

molecules as tetrahedra forming approximately four hydrogen bonds on average has been widely accepted.

Generally, proton transfer is considered in the case of the H_3O^+ ion in the Grotthuss mechanism³⁷ involving Eigen-Zundel-Eigen complexes. The mechanism by which the neighboring water molecule in the Eigen complex gets close to the H_3O^+ ion to form the Zundel complex involves both first and second shell water molecules surrounding the H_3O^+ ion^{3, 5, 16, 17, 20, 27, 38}, with multiple hydrogen bond rearrangements^{8, 11}.

Of course, the initial formation of the H_3O^+ ion is either intentionally introduced into solution or is the result of autoionization of the water molecule to form the H_3O^+ and OH^- ion pair. Geissler et al. have previously discussed autoionization in water using ab-initio calculations³⁹. However, rapid recombination of the ion pair in a neutralization event dominates⁴⁰ and leads to the estimate that recombination is over 1000 times more likely than separation and stabilization of the ion pair⁴¹. The hydrogen bond network plays an important role in formation and stabilization of the H_3O^+ and OH^- ion pair via separation, with a strong dependence on a H-bond chain that enables rapid transport of the proton away from the OH^- ion via structural diffusion of the H_3O^+ complex. Since separation is a rare event, the role of the H-bonding between the donor and acceptor on dissociation of the water molecule and subsequent rapid recombination is important.

Using AIMD calculations, Kühne and Khaliullin showed that the donated hydrogen bonds of a typical water molecule have unequal electronic charge transfer on short timescales⁴². Averaged over hundreds of femtoseconds, a typical molecule's two donated hydrogen bonds are nearly equal; however, at the sub-100 femtosecond timescale, molecular vibrations and librations strengthen one bond at the expense of the other. Ab initio calculations have shown that, even for short linear hydrogen bonds, the electrostatic contribution to hydrogen bonding energy dwarfs that of electronic charge transfer by a factor of 5 to 6^{43, 44}. Together, these results suggest that the absence of charge transfer in a hydrogen bond should not be interpreted as a lack of hydrogen bonding and raise the question of exactly what constitutes a hydrogen bond.

The most common definitions of a hydrogen bond have been geometric (e.g., requiring that $r_{\text{OO}} < 3.5 \text{ \AA}$ and $\theta_{\text{OOH}} < 30^\circ$) and energetic (based on a cutoff in the intermolecular potential energy); hybrid definitions that are part geometric and part energetic have also been used. Despite their differing inclusiveness, these definitions yield similar structural and dynamical results^{45, 46}. Because the hydrogen bonding interaction is predominantly electrostatic, and therefore continuous with no natural cutoff, the imposition of a geometric or energetic cutoff necessarily introduces discontinuities into the

resulting analysis. An ideal characterization of hydrogen bonding should capture the whole continuum of first-neighbor interactions and recognize a subset of these, for which electron charge transfer does occur, as the strongest. Henchman et al. proposed a topological definition of the hydrogen bond in which every hydrogen forms a single bond to its closest non-covalent oxygen, provided that another stronger bond does not exist between the two molecules⁴⁵. This definition, lacking any arbitrary cutoffs, was employed in their MD studies based on the TIP3P, SPC/E, TIP4P, and TIP4P/2005 water models^{26, 32, 45}.

Using their topological hydrogen bond definition, Henchman et al. found that 60% to 70% of molecules assume a tetrahedral coordination and that 0.8% to 2.3% of the hydrogens are dangling.⁴⁵ They also found that bifurcated bonds, which can switch to a different acceptor with little or no energy barrier, occur when a hydrogen's current acceptor is more coordinated than its next-nearest acceptor³².

The mechanism by which a proton switches from one acceptor to another has been traditionally described as rotational diffusion occurring over many small steps, but a major development over the past decade has been the large amplitude angular jump model of Laage, et al.⁴⁷⁻⁵⁰. According to the large-amplitude jump model, hydrogen bonds switch acceptors predominantly via large-amplitude, concerted motions, as opposed to gradual small-step diffusive rotation. As a new acceptor moves in from the second coordination shell, the proton's original acceptor moves away concertedly, and the proton makes a large jump to the new acceptor over an average angle of 68°. This model has been invoked to explain the behavior and the frequency-dependence of angular correlation functions, which measure the timescale on which molecular reorientations occur⁴⁷. Experimental angular correlation functions have been obtained from pump-probe spectroscopy experiments^{51, 52}, in which protons in a specific OH stretch frequency range are excited with a pulse, so that subsequent probe pulses can monitor the rate at which this excited population reorients. Given that a proton's vibrational frequency correlates with its hydrogen bond strength⁵¹, this provides an experimental means of correlating hydrogen bond strength with reorientation times.

Angular correlation functions exhibit a rapid decay over times shorter than a picosecond and a slow decay on a picosecond timescale. Laage, et al. attribute the fast decay to librational motions within a cone whose radius is a function of the hydrogen bond strength^{50, 53}. They propose that large angular jumps associated with hydrogen bond switches are the mechanism of reorientation on long timescales, and postulate that the probability of such a jump occurring is independent of the hydrogen bond strength, because it depends only on the availability of a second-shell acceptor. For this reason, they conclude that only short-timescale reorientation rates depend on hydrogen bond strength. In a computational study of dilute HOD in D₂O, Laage, et al. have calculated angular correlation functions

for five different ranges of OH stretch frequencies using a rigid water interatomic potential and calculated the OH stretch frequency using a perturbation method and concluded that all H-bond frequency ranges decayed at the same rate on long timescales⁵³.

Further investigation of the relation between the frequency, structure, reorientation rates of H-bonds and proton transfer using an all-atom dissociative interatomic potential that inherently allows for OH stretch frequencies and proton transfer based on local structure is warranted. Using the definition developed by Henchman et al.⁴⁵ in the current study, the bonds of a system are categorized based on their strengths relative to other bonds donated by the proton's donor molecule and accepted by the proton's acceptor molecule. That is, the local structure around the acceptor molecule is included in the categorization of the bonds, inherently including the role of second shell waters on H-bonding. The reactive all-atom potential developed by Mahadevan and Garofalini is used⁵⁴. This potential is dissociative and non-rigid and enables analysis of the changes in the bond lengths and angles for specific structural elements that would not be available with rigid water potentials. It has been shown that allowing molecules to polarize has a substantial effect on the strength, stability, and cooperativity of water's hydrogen bonds⁵⁵. This potential has been shown to reproduce a variety of bulk water properties, such as the structure, heat of vaporization, and frequency spectrum of bulk water⁵⁴, dissociative reactions and hydroxylation on the silica surface⁵⁶, the anomalous thermal expansion of nanoconfined water^{57, 58}, and diffusion of water through nanoporous glass⁵⁹. As a dissociative potential, proton transport in bulk water²⁷ and at water-silica interfaces⁶⁰ were analyzed, all with results consistent with experimental data or ab-initio calculations. In the analysis of proton transfer from H_3O^+ ions, the Eigen-Zundel-Eigen mechanism is observed, similar to ab-initio and experimental studies. An activation barrier of proton transport in the Zundel complex in bulk water of 0.8 kcal/mol at an O-O spacing of 2.4\AA ²⁷ was observed, similar to the value of 0.6 kcal/mol obtained by Marx in DFT calculations⁹. Using this potential, Hofer showed that the diffusion coefficient of the hydronium complex is 30% more accurate than the touted MS-EVB3 model of proton transport²⁴, although both are lower than the experimental result.

In addition, since this reactive potential allows for proton transfer consistent with ab-initio calculations and experiment²⁷, the relationship between proton transfer and hydrogen bond type and lifetimes can be analyzed. Proton transport (PT) has been well studied using both computational and experimental methods^{1, 7, 9, 10, 14, 16, 24, 34, 38, 61} and is usually associated with the structural diffusion of the hydronium complex. PT in the H_3O^+ complex in water occurs via a Grotthuss mechanism involving Eigen (H_9O_4^+) and Zundel (H_5O_2^+) complexes, in which the H_3O^+ ion with 3 H-bonds to first shell waters in the Eigen complex eventually associates with one of the waters to form a Zundel complex, at

which point the proton can transfer, with reversion to a new Eigen complex with the new H_3O^+ ion. Marx showed that the barrier to PT in the Zundel complex decreases with decreasing O^*-O spacing (where O^* indicates the hydronium oxygen)^{5,9}; similar results were observed in MD simulations²⁷ using the potential used here. The MD simulations showed continuous and intermittent lifetime autocorrelation functions of 30 bulk water systems containing either 792 or 4000 water molecules (plus one H_3O^+ ion in each system) on the femtosecond scale (consistent with proton rattling) and the picosecond scale (consistent with proton transfer), and a long-time tail at times greater than 100 ps in the intermittent lifetime autocorrelation function that fit the $t^{-3/2}$ power law related to diffusion²⁷. These previous simulations showed that the shortest-lived O^* (< 200 fs) that are a result of proton rattling exhibit an O^*-H first peak with a large longer-distance shoulder that is indicative of the Zundel complex as the proton fluctuates between both oxygens; this shoulder in the first O^*-H peak decreases with increase in the lifetime of the O^* (hydronium) as the proton remains close to its O^* for more time in the Eigen complex²⁷. The simulations also show that proton rattling in the H_3O^+ complex is related to a presolvation model, similar to ab-initio results⁶².

Given the applicability of this reactive potential to produce simulation results consistent with a variety of experimental and ab-initio data of water, including proton transport, application to a study of hydrogen bond lifetimes and auto dissociation via proton transfer in neat water is warranted using the more general Henschman definition of the hydrogen bond. Most importantly, the role of the H-bond state of the acceptor oxygen on H-bond lifetimes of the central oxygen's proton and the effect on proton transfer causing auto dissociation is evaluated.

Computational Procedure

The reactive potential⁵⁴ used in this simulation comprises a two-body term and a three-body term and allows for dissociation of the water molecule. The two-body term, which acts on atom pairs, models each atom as a point charge (q_i) with a surrounding diffuse charge ($q_i^d = -q_i/4$). Coulombic forces act on all pairs of atoms, Pauli repulsion forces act on OO and OH pairs, and a London dispersion force acts on OO pairs:

$$U_{2-body} = U_{qq} + U_{q^d q^d} + U_{qq^d} + U_{q^d q} + U_{rep} + U_{disp} \quad (1)$$

where,

$$U_{qq}(r_{ij}) = \frac{q_i q_j}{r_{ij}} \operatorname{erfc}\left(\frac{r_{ij}}{\beta}\right) \quad (2)$$

$$U_{q^d q^d}(r_{ij}) = \frac{q_i^d q_j^d}{r_{ij}} \operatorname{erf}\left(\frac{r_{ij}}{2\xi_{ij}}\right) \operatorname{erfc}\left(\frac{r_{ij}}{\beta}\right) \quad (3)$$

$$U_{qq^d}(r_{ij}) = \frac{q_i q_j^d}{r_{ij}} \operatorname{erf}\left(\frac{r_{ij}}{\sqrt{2}\xi_{ij}}\right) \operatorname{erfc}\left(\frac{r_{ij}}{\beta}\right) \quad (4)$$

$$U_{q^d q}(r_{ij}) = \frac{q_i^d q_j}{r_{ij}} \operatorname{erf}\left(\frac{r_{ij}}{\sqrt{2}\xi_{ij}}\right) \operatorname{erfc}\left(\frac{r_{ij}}{\beta}\right) \quad (5)$$

$$U_{rep}(r_{ij}) = A_{rep}^{ij} \frac{\operatorname{erfc}(z_{ij})}{z_{ij}} \left(z_{ij} = \frac{r_{ij}}{2\xi_r^{ij}} \right) \quad (6)$$

$$U_{disp}(r_{ij}) = \frac{-c_6^{ij}}{r_{ij}^6} \quad (7)$$

summed over all pairs, $i > j$.

The intramolecular three-body term acts on all HOH triplets j, i, k for which $r_{jk} < 1.6 \text{ \AA}$ and $r_{ik} < 1.6 \text{ \AA}$.

$$U_{3-body}(r_{ij}, r_{jk}, \theta_{jik}) = \lambda \exp\left(\frac{\gamma}{r_{ij}-r_0} + \frac{\gamma}{r_{ik}-r_0}\right) [\cos(\theta_{jik}) - \cos(\theta_0)]^2 \quad (8)$$

The two-body and three-body parameters are given in Table 1.

The simulations were conducted using an isothermal-isobaric ensemble (NPT) bulk water system, consisting of 27,000 molecules with periodic boundary conditions in all three dimensions. The temperature and pressure were fixed at 298K and 1atm, respectively. The simulations were performed using the Wolf summation⁶³, with β equal to $4.46 \times 10^{-8} \text{ \AA}$, a cutoff (R_c) of 10 \AA , and a timestep of 0.1fs. Once initialized, the system was run for 200ps, followed by an additional 100ps run, with configurations saved every femtosecond for subsequent analysis (allowing for 100,000 configurations). All structural data were averaged over these configurations.

The topological definition of the hydrogen bond is instantaneously determined at a each configuration as follows. At time t , the m th nearest oxygen atom to hydrogen H_i is labeled $O_m(H_i, t)$, and the pair's HO distance is referred to as $r_m(H_i, t)$. When the time is impertinent, we shall simply

write $O_m(H_i)$ and $r_m(H_i)$. $O_1(H_i)$ is the hydrogen's covalently bonded oxygen; if H_i forms a hydrogen bond, then $O_1(H_i)$ is said to donate a hydrogen bond to $O_2(H_i)$ through H_i . Qualitatively, we refer to a hydrogen bond as linear if $O_2(H_i)$'s role as H_i 's acceptor is unambiguous due to $r_2(H_i)$'s being significantly shorter than $r_3(H_i)$ for an extended period of time. If $O_2(H_i)$'s role as H_i 's acceptor is ambiguous, the bond is referred to as bifurcated. These descriptions are qualitative and represent the endpoints of a continuum of bonding geometries. To quantify this notion, we define a delta function as the difference between r_3 and r_2 as:

$$\delta(H_i) = r_3(H_i) - r_2(H_i), \quad (9)$$

which is large for linear bonds and small for bifurcated bonds. One could arbitrarily use a value of $\delta = 0.9$ as a cutoff, with smaller values for bifurcated bonds and larger values for linear bonds. The rationale will be shown below regarding the results for the δ values of the different bonds.

If H_i does not form a strong interaction with any acceptor, then H_i is referred to as a dangling hydrogen. According to the topological hydrogen bond definition, every hydrogen H_i forms a hydrogen bond between $O_1(H_i)$ and $O_2(H_i)$, unless another hydrogen H_j forms a stronger bond between $O_1(H_i)$ and $O_2(H_i)$. As shown by Henchman et al. using the rigid TIP4P/2005 potential⁴⁵, and corroborated by our data, the latter condition accurately identifies hydrogen atoms which, at that instant, do not associate with an acceptor. Henceforth, we shall refer to H_i as bond-forming if $B(H_i)=1$ and dangling if $B(H_i)=0$, where:

$$\begin{aligned}
 B(H_i) = 0, & \text{ if there exists a hydrogen } H_j \text{ such that } r_2(H_j) < r_2(H_i) \text{ and} \\
 & \text{one of the following two conditions holds:} \\
 & \text{(1) } O_1(H_j) = O_1(H_i) \text{ and } O_2(H_j) = O_2(H_i) \\
 & \text{(2) } O_1(H_j) = O_2(H_i) \text{ and } O_1(H_i) = O_2(H_j) \\
 & = 1, \text{ otherwise}
 \end{aligned} \quad (10)$$

Equation 10 indicates that there are 2 H's to consider: H_i and H_j and consider if H_i is bond forming. First, r_2 denotes the distance of the H-bond. $B(H_i)$ equals zero if H_j has a closer r_2 bond than H_i plus one of the 2 additional conditions as shown in figure S1 in the supplementary file. Briefly, the two additional conditions mean: (1) both H_i and H_j are covalently bonded to the same O_1 and they are H-bond interacting with the same O_2 , which means that H_j has a closer H-bond to O_2 than H_i , thus H_i is dangling since its closest non-covalently bonded O is O_2 ; or (2) the oxygen to which H_j is covalently bonded (H_j 's O_1) is also the oxygen to which H_i is H-bonded (H_i 's O_2) and the oxygen to which H_i is covalently bonded (H_i 's O_1) is also the oxygen to which H_j is H-bonded (H_j 's O_2).

With respect to oxygen O_i , $n_{\text{Accepted}}(O_i)$ is the number of bond-forming protons for which $O_2(H_j)=O_i$, $n_{\text{Donated}}(O_i)$ is the number of bond-forming protons for which $O_1(H_j)=O_i$, and $n_{\text{Dangling}}(O_i)$ is the number dangling protons for which $O_1(H_j)=O_i$. We consider the coordination state of any oxygen in a molecule to be fully characterized by the three integers n_{Accepted} , n_{Donated} , and n_{Dangling} . O_i 's number of covalent hydrogens is $n_{\text{Donated}}(O_i)+n_{\text{Dangling}}(O_i)$, which is two for a neutral water molecule and one or three for a hydroxide or hydronium ion, respectively.

The hydrogen bonds donated and accepted by every molecule were ranked according to r_2 . This was done by listing the bonds donated and accepted by every molecule O_i and sorting them by ascending r_2 . The rank of H_i is $D_m A_n$ if H_i has the m th shortest r_2 of all the H-bonds donated by $O_1(H_i)$ and if it has the n th shortest r_2 of all the H-bonds accepted by $O_2(H_i)$, where $1 \leq m \leq n_{\text{Donated}}(O_1(H_i))$ and $1 \leq n \leq n_{\text{Accepted}}(O_2(H_i))$. A bond's rank therefore reflects its instantaneous strength relative to its donor's other donated bonds and relative to its acceptor's other accepted bonds. The correlation between rank and bond strength can be seen in vibrational spectra, which we obtained through a Fourier transform of the velocity autocorrelation functions for the protons of each rank. Our velocity autocorrelation functions were calculated according to the following formula:

$$c_v(t) = \frac{\langle \vec{v}(H_i, t_0) \cdot \vec{v}(H_i, t_0 + t) \rangle}{\langle \vec{v}(H_i, t_0) \cdot \vec{v}(H_i, t_0) \rangle} \quad (11)$$

Where $\vec{v}(H_i, t)$ is the instantaneous velocity vector of proton H_i at time t , and \cdot is the dot product. These were calculated for $0 \leq t \leq 500$ fs. The averages are taken over all protons assuming a given rank at time t_0 , with 95,500 starting t_0 configurations, each separated by 1fs and carried out for 0.5ps.

Angular correlation functions show the rate at which molecules rotate from their original orientations and, in particular, second-order angular correlation functions are proportional to anisotropy decay functions obtained through ultrafast IR experiments⁵¹. We obtained first-order and second-order orientational correlation functions (c_n) for bonds of each rank using the formula:

$$C_n = \langle P_n(\vec{r}_0 \cdot \vec{r}_t) \rangle \quad (12)$$

where P_n is the n th-order Legendre polynomial and r is a unit vector attached to the bond. In our calculations, r it is the normalized covalent OH vector. n is equal to 1 and 2 for first-order and second-order correlation functions respectively. $\vec{r}_0 \cdot \vec{r}_t$ is the cosine of the angle between the OH vector's

initial orientation (t_0) and its orientation after time t has elapsed. The average is taken over all protons which, at time t_0 , formed a hydrogen bond of a given rank.

The system's hydrogen bond lifetimes and bond rank lifetimes were characterized using continuous lifetime autocorrelation functions, $C_C(t)$, which were calculated for all H-bonds as well as for each rank. These were defined with respect to a pair of step functions $f(H_i, t_0)$ and $F(H_i, t_0, t)$. $f(H_i, t_0)$ equals 1 if some condition is satisfied by proton H_i at time t_0 , and 0 otherwise; $F(H_i, t_0, t)$ equals 1 if the same condition is satisfied continuously from time t_0 to t_0+t , and 0 otherwise. The correlation functions are of the form:

$$C_C(t) = \frac{\langle f(H_i, t_0)F(H_i, t_0, t) \rangle}{\langle f(H_i, t_0) \rangle} \quad (13)$$

The averages are taken over all protons meeting the $f(H_i, t_0)$ criteria, and the t_0 time-point corresponds to the configuration where H_i first meets the $f(H_i, t_0)$ criterion. In the case of the h-bond lifetime autocorrelation function, $f(H_i, t_0) = B(H_i, t_0)$ and $F(H_i, t_0, t) = 1$ if H_i continuously forms a bond between $O_1(H_i, t_0)$ and $O_2(H_i, t_0)$ from time t_0 to t_0+t . This was calculated for $t \leq 30$ ps for all bond-forming protons regardless of rank. In the case of rank lifetime autocorrelation functions, $f(H_i, t_0) = 1$ if H_i assumes a particular rank at time t_0 , and $F(H_i, t_0, t) = 1$ if H_i continuously forms an h-bond between $O_1(H_i, t_0)$ and $O_2(H_i, t_0)$ with the same rank from time t_0 to t_0+t . It is calculated for each rank for $t \leq 3$ ps, and expresses the probability that a hydrogen bond which first assumed a given rank at time t_0 maintains it continuously to time t_0+t .

Results and Discussion

The observed oxygen coordination states are shown in Table 2; states with probabilities smaller than .001% were omitted from the table. As expected, the majority of molecules (67%) donate and accept two hydrogen bonds, while significant minorities accept one or three hydrogen bonds. This is comparable to the statistics calculated by Henchman et al. at 298K using the topological hydrogen bond definition⁴⁵. They found that 60% of molecules had tetrahedral coordinations in TIP3P and 70.9% in TIP4P/2005, with SPC/E and TIP4P falling in-between. DiStasio et al.⁶⁴ obtain a concentration of double donor-double acceptor totaling ~69% at the DFT level using PBE+Tkatchenko-Scheffler density dependent van der Waals term. The use of the hybrid PBE0 version with the added vdW terms at higher temperature lowers the double donor-double acceptor value to ~50%.

Neutral double donors account for 98.6% of our system, and neutral molecules with one donor (and hence, one dangling hydrogen) account for most of the remainder. Compared to neutral double-donors, neutral single-donors have a similar n_{Accepted} distribution which is shifted toward fewer accepted bonds. Because our system is neutral bulk water, the numbers of hydroxide and hydronium ions are equal at all times, with hydroxide ions marginally more likely to possess a dangling hydrogen (causing the slightly lower total of single donors). The presence of the non-H-bonded proton on the hydroxide ion is consistent with previous data³⁴.

Hydrogen bond ranks with their associated probabilities are listed in Table 3; ranks with a probability of less than 0.1% are omitted. D_1A_1 , D_2A_1 , and D_1A_2 , whose bonds are almost exclusively linear, account for 64.2% of the system's hydrogen atoms. D_2A_2 and D_1A_3 , which contain both linear and bifurcated bonds, account for an additional 28.3% of the hydrogens. Therefore, we establish 64.2% and 92.5% as the lower and upper limits for the portion of protons which form linear hydrogen bonds, with 83% being our estimate from the delta distributions.

Henchman et al. found that dangling hydrogens at 298K constitute 2.3% (TIP3P), 1.4% (TIP4P), 1.1% (SPC/E), and 0.8% (TIP4P/2005) of their respective systems⁴⁵. Our value of 0.7% is the lowest of any potential yet reported; our potential's molecular flexibility may result in fewer dangling hydrogens because it permits the donor molecule to bend while preserving a strained bond. Of our system's dangling hydrogens, 55% are donor type (type-D) and 45% are acceptor type (type-A); by contrast, Henchman, et al. observed 37.5% type-D and 62.5% type-A dangling hydrogens in their TIP4P/2005 system. The higher fraction of type-D dangling hydrogens in the reactive all-atom potential used here compared to TIP4P/2005 is likely explained by the contraction of the dangling hydrogen's covalent bond, which in our potential, brings its positive charge closer to the oxygen. (This is seen in the structural relationships shown below.) This allows the molecule's other covalent OH bond to stretch more, strengthening its hydrogen bond with O_2 , allowing for a more acceptable energetic relation that would be missing with rigid water potentials.

The system's overall O2-O1-H hydrogen bond angle and r_2 distance distributions, shown in figure 1a and 1b, respectively, can be compared to experimental data obtained through NMR⁶⁵. Our angle distribution matches their 27° C distribution very closely. While the shape and mode of our r_2 distribution match theirs well, our distribution has a smaller peak and more spread than theirs at 27° C, with our r_2 distribution falling between their 50° C and 80° C distributions. Their ab-initio DFT calculations put 91.7% of r_2 distances less than 2.4Å, and our results similarly indicate that 91.1% of protons have an r_2 distance less than 2.4Å.

Figure 2 shows a set of structural relationships among the bond ranks and elucidates the nature of dangling hydrogens. Figure 2 shows the HO PDF for the first four H-O distances, with the r_3 and r_4 distances falling within the same peak. The shifts in the HO distances among the different ranks seen in figure 2 are delineated more fully in figures 3a-d. Recall that r_i denotes the distance between the proton and the i^{th} O neighbor. The r_1 distributions (3(a)) show that lower-ranked bonds, in which the acceptor is closer, have more polarized covalent bonds, whereas the dangling hydrogens have the least stretched covalent bonds (the effect of these different OH distances for r_1 on OH vibrations is discussed later with respect to figure 6).

There is substantial variation among the ranks' r_2 distributions, with that of dangling hydrogens occurring at a distance comparable to the r_3 distributions and consistent with the r_1 distance being shorter for these dangling protons. While the r_1 distances fall within a small range than the r_2 distances, there is a clear association that longer r_2 distances correlate with shorter r_1 distances. The D_1A_1 , D_2A_1 , and D_1A_2 distributions have r_2 peaks between 1.72Å and 1.88Å and a negligible fraction beyond 2.3Å, from which it can be concluded that these molecules donate and accept at least one strong hydrogen bond.

The r_3 , r_4 peaks in figures 3c and 3d help to elucidate the character of weaker bonds found in D_2A_2 , D_1A_3 , and higher ranks. The 4th O is only slightly farther from the proton than the 3rd O, but its distribution for the different ranks is more uniform and narrower than in the case of the r_3 peaks. While these ranks do capture a subset of linear geometries, the overall trend is slightly shorter r_3 and r_4 distances compared to the strictly linear ranks. Notice that for short distance side of the r_3 curves, the bond's A ranks cluster in pairs of A1, A2, and A3. Table 4 provides the probability that a hydrogen's O3 is bonded to either O1 (the proton's covalently bonded O), O2 (the first shell water), neither or both for each bond rank and is ordered from top to bottom by decreasing probability of O3 bonded to O1, which also results in increasing probability of O3 bonded to O2 (excluding dangling bonds). This ordering also results in the more linear bonds at the top of the table and the more bifurcated bonds at the bottom, which is consistent with the O_2 - O_1 -H angles and δ distributions to be discussed below.

The O_1 - O_2 distance distributions, shown in figure 4, show that nearly every molecule donates and accepts at least one bond with $r_{O_1O_2} < 3.2\text{\AA}$. The O_1 - O_2 distance distribution for dangling hydrogens is characteristic of a pair between which another strong hydrogen bond exists, and their O_2 - O_1 -H angle distribution, shown in figure 5a, shows a significant deviation from linear geometry. The O_2 - O_1 -H angle distributions also show that almost every molecule donates and accepts at least one bond with an OOH angle less than 35°. These O_2 - O_1 -H angle distributions are consistent with previous work

showing that hydrogen with a short hydrogen bond length (strong hydrogen bond strength) must have a restricted distribution of OOH angles^{50, 66}.

These trends show that bond-forming hydrogens compensate for an energetically unfavorable r_2 by moving closer to O_3 and O_4 . This is not true for dangling hydrogens, which have longer r_2 , r_3 , and r_4 distances than bond-forming hydrogens. This implies that when the local structure precludes H_i from associating with $O_2(H_i)$ and other proximal oxygens, contraction of r_1 and strengthening of $O_1(H_i)$'s other hydrogen bond occurs.

The two peaks in the O_3 - O_1 -H angle distribution shown in figure 5b correspond to situations where O_3 is H-bonded to O_2 (the lower-angle peak) or O_1 (the higher-angle peak). This interpretation is supported by the data shown in figure 5c, which shows the cause of the dual peak in figure 5b. O_3 - O_1 -H angle is lower for O_3 H-bonded to O_2 than for O_3 H-bonded to O_1 . O_3 hydrogen bonded to both O_1 or O_2 or to neither fall between the other peaks. Dangling hydrogens as well as D_2A_3 and D_1A_3 bonds have the smallest O_3 - O_1 -H angles, while linear bonds tend to have the widest. As shown in table 4, higher ranks have a strong trend of O_3 being bonded to O_2 (via the H) rather than O_1 , which results in a smaller O_3 - O_1 -H angle and a more bifurcated geometry. As with r_3 and r_4 , the distribution depends strongly on the bond's A rank for small O_3 - O_1 -H angles, with a higher A rank resulting in a more bifurcated geometry.

The δ distributions (the difference between the r_3 and r_2 distances) shown in figure 6 most clearly illustrate a rank's relative populations of linear and bifurcated bonds and the important distinction between first and second shell waters. D_1A_1 , D_2A_1 , and D_1A_2 clearly only consist of linear bonds, with $\delta=0$ having zero probability. D_2A_2 and D_1A_3 have populations of bifurcated bonds in addition to linear bonds, and for D_2A_3 and D_2A_4 we see a large predominance of bifurcated bonds. Because bifurcated bonds do associate with an acceptor, their δ distributions are farther from zero than those of dangling hydrogens. There is a relatively large population near $\delta=0$ for several ranks that, from Table 3, make up over 8% of the system. From Table 4, we see that these same ranks show a significant concentration of the O_3 water H-bonded to the O_2 water, indicating that O_3 is in the central water's second shell. These data provide an important indication of another water molecule from a central water's second shell moving into its first shell waters, similar to the ab-initio calculations presented by DiStasio et al.⁶⁴.

Figure 7 shows the high frequency (bond stretching) peak in the vibrational spectrum of the protons as a function of proton rank. The dangling protons have the highest frequency peak consistent with the aforementioned shortest HO covalent bond length shown in figure 3b. Those protons with stronger hydrogen bonds have commensurately lower vibrational frequencies.

The continuous hydrogen bond autocorrelation functions of figure 8a were calculated for all newly formed hydrogen bonds. The semi-log plot shows that simple exponential decay occurs for lifetimes longer than about 1ps, with a time constant of 2.1ps. The high decay rate for short-lived bonds occurs because the majority of newly formed bonds are unstable, while a small subset of them are able to stabilize as linear bonds. This subset exhibits simple exponential decay, as observed for bond lifetimes longer than 1ps. This is consistent with the results of mid-IR pump-probe spectroscopy performed on dilute HDO in D₂O, in which high-frequency bonds were found to reorient through a fast and a slow process, whereas the lowest-frequency bonds reorient through only the slow process.⁶⁷

The continuous rank autocorrelation functions shown in figure 8b show the probability that a hydrogen bond, which first assumed a given rank at time t_0 , maintains this rank continuously until time $t_0 + \Delta t$. (The ‘lifetime’ for the Dangling bond is, of course, not the lifetime of a hydrogen bond, but is rather the lifetime of the dangling bond state.) While the overall hydrogen bond continuous lifetime correlation function lasts for 2.1 ps, the specific rank lifetimes are much shorter-lived. These rank lifetime functions decay to 0.5 in approximately 20fs, as shown in figure 8c; this is shorter than the timescale of intramolecular vibrations and librations. This shows that a large fraction of molecules has nearly symmetric donated and accepted bonds that change rank with small intermolecular and intramolecular motions. For Δt exceeding about 20fs, the decay of these functions is driven primarily by molecular vibrations and librations, which tend to instantaneously strengthen one bond at the expense of others, which truly shows up at times greater than ~ 300 fs in figure 8b. D_1A_1 decays the slowest due to a small fraction of its bonds (about 1% in 8b) that, due to a highly asymmetric local bonding environment, maintain their D_1A_1 status over an entire vibration/libration period. D_1A_2 and D_2A_1 decay to less than 1% over a vibration/libration period, while D_2A_2 and D_2A_3 decay more slowly as a result of weak and bifurcated bonds which never get promoted to higher ranks over a vibration or libration period.

Figure 9 shows rank-based (a) first-order and (b) second-order angular correlation functions, with the associated time constants shown in table 5. At times less than 25fs, all ranks decay at the same rate; however, the extent of the initial decay is strongly rank-dependent. As previously argued^{48,53}, this short-time decay is due to librational motion of protons confined to a potential well. As shown in figure 10a, all ranks liberate with a nearly identical distribution of angular velocities. However, the ranks consisting of weaker bonds have larger-amplitude librations with longer periods. The increase in the angular correlation functions from around 25fs to 75fs is due to librating protons reaching the end of their angular range and “bouncing back” toward their initial orientations, as previously observed with rigid water molecules⁵³.

While pump-probe spectroscopy and a simulation have indicated that the rate of orientational decay beyond 1.5ps is independent of hydrogen bond strength^{51, 52, 67}, we find a small dependence of the time constant on rank, with a 7% difference between the fastest long-time reorientations (dangling, with $\tau_1=4.59\text{ps}$) and the slowest (D1A1, with $\tau_1=4.89\text{ps}$). To obtain time constants for the long-time orientational decay, we used the region from 3ps to 4ps; as libration-associated decay occurs on a sub-picosecond timescale, a 3ps delay is more than sufficient to avoid any influence from librations on the long-timescale decay constants. Over the 3ps to 4ps range, every first-order and second-order angular correlation function fit an exponential decay curve very closely. As shown in Table 5, the relationship between τ_1 and rank mirrors the structural relationships, with stronger bonds having slower long-timescale decay rates.

Figure 10b shows the mean angular displacement over time for protons of each rank. Also plotted is the line $\Delta\theta = \langle \omega \rangle t$, representing the angular displacement of a freely rotating molecule whose angular velocity is the modal angular velocity corresponding to the peak of the distributions in figure 10a. We determined $\langle \omega \rangle$ to be $.93^\circ/\text{fs}$ and estimated the half-radius of each rank's librations based on the intersection of this line with the respective angular displacement curves; these estimates are shown in Table 5. Compared to the librational half-radius of D1A1 protons (14.2°), that of D2A3 is wider by a factor of two, and that of dangling protons is wider by a factor of three. These half-radii agree closely with those obtained by Laage, et al. as a function of OH stretch frequency^{50, 53}.

A summary of rank-associated structural and dynamical trends is shown in Table 6.

Autoionization via Proton Transfers

Autoionization via proton transfers (PT) were observed in these simulations because of the use of the dissociative interatomic potential function that allows for such transfers in a manner consistent with ab-initio calculations⁶⁰. While PT is generally considered with respect to the structural diffusion of the H_3O^+ ion, we use it here to also include the transfer of the proton in autoionization. The number of protons that transferred between oxygens over the 100ps analysis run was small given the number of waters in the system (27,000 waters) and the number possible transfers based upon the number of time steps (1.0×10^6). Considering all proton transfers that began and ended within the timeframe of the analysis, there were 1100 transfer events over the entire trajectory, in which 428 molecular pairs were involved. All of these transfers occurred when the proton was ranked D1A1. From figures 3a and 3b, the overall D1A1 have a $\sim 2.5\%$ longer covalent bond (r_1) and $\sim 3.5\%$ shorter H-bond (r_2) than the overall average for water (The r_2 decreases more-so due to a decrease in the average O1-O2 spacing as

shown in figure 4.). This implies that the protons that transferred were those with the weakest covalent bond and strongest H-bond to the accepting water molecule from the donor. In detail, the D1A1 that showed autodissociation PT had an average covalent bond length (r_1) that was $\sim 6\%$ longer than the average in water. The greatest change in the increase in the covalent bond length occurred within the last 50fs prior to the PT event. Figure 11a shows the median r_1 for all D1A1 protons (dotted line, which is not time dependent) and the median r_1 for those D1A1 that showed proton transfer (solid line) as a function of time prior to the PT event (which is at time=0 on the graph). Clearly, those D1A1 that showed PT had a longer covalent bond length than even the overall D1A1. Oscillations in the distance begin within 50fs of the PT event. These are conversely mimicked by the H-bond distance (r_2) as a function of time shown in 11b. Figure 11b also shows the O1-O2 spacing at these D1A1 that shows an increase in distance just prior to the final approach for proton transfer. The importance of such results that show that auto dissociation via proton transfer occur in species that have a weak covalent bond and stronger H-bond is consistent with results shown by Reischl et al. who concluded that a strong electric field generated by local water molecules initiates the dissociation of the water molecule⁶⁸. The result is also consistent with previous studies indicating that hydronium ions exchange protons with the strongest H-bond of the hydronium's three acceptors³. Reischl et al. discussed the role of the central water having more accepting bonds that relates to large electric fields that enhance dissociation and autoionization⁶⁸. They report that an average number of H-bonds with strong fields was 4.27 per molecule. The average number of H-bonds on the donating oxygens at the time of proton transfer in the simulations shown here is 4.32 per molecule, in excellent agreement with data from Reischl et al. The acceptor oxygens had an average of 3.68 H-bonds per molecule at the time of transfer.

Almost all (99.7%) of these transfer events involved dissociation and proton transfers (or autoionization events) that formed transient $\text{OH}^-/\text{H}_3\text{O}^+$ pairs that rapidly relaxed back to their neutral molecular states (A-B-A events, where the letters stand for oxygens in the transfer, which are otherwise O_1 and O_2 with regard to the proton and labeling above). 98.2% of the transfers (A to B to A) occurred within femtoseconds, consistent with short-time proton rattling. The existence of such transient $\text{OH}^-/\text{H}_3\text{O}^+$ pairs that form between auto-ionizing waters has been previously observed in CPMD simulations³⁹. The other 1.8% occurred within picoseconds. There were also seven A-B-C-B-A chains and one A-B-C-D-C-B-A chain, each relaxing to their initial neutral molecular states (again, each letter corresponds to a specific oxygen in the chain, so A-B-C-B-A involves 3 oxygens, A, B, and C).

Four separate examples of A-B-A autoionization events are shown in figure 12. The red line indicates the time of the existence of a H-bond for each particular A-B pair (2 neutral water molecules), with the time axis starting at the onset of the H-bond for each event shown. The blue line

(or dot) indicates the lifetime of the proton on the original acceptor molecule (B here), in which the start of the blue line is the instant of proton transfer from A to B (creating OH^- and H_3O^+ ions, respectively) and the end of the blue line is the reverse transfer from B to A, reinstating the original neutral water molecules. Event 1 in the figure is the most prevalent type event in the system, occurring in 78% of the autoionization cases that neutralized within 50 fs (indicative of the blue dot which is enlarged in the time domain so as to be viewed in the graph). 10% of the autoionizations occurred in a manner shown in event 2, in which the autoionizations have $\text{OH}^-/\text{H}_3\text{O}^+$ lifetimes ranging from 200 fs to 3 ps; event 2 had ~ 5 ps H-bond and a 631 fs autoionization state (proton on B, forming the $\text{OH}^-/\text{H}_3\text{O}^+$ ion pair). Event 3 shows a 622 fs autoionization within a 1ps H-bond lifetime. Event 4 represents a significant outlier of events, in which only 6 autoionized pairs break their H-bonds between A and B prior to reinstating the H-bond and the return PT from B back to A. Of these 6 outliers, the H-bond is broken for less than 10fs for 3 of them, less than 241 fs for 2 (the 241 fs case is shown in Event 4 in the figure), and 1 at 2 ps.

The H-bond lifetime for all cases involving proton transfers were longer than the H-bond lifetime of all non-PT molecular pairs as shown in figure 13. The figure shows the continuous H-bond lifetime autocorrelation function for all protons that transferred from their original covalently bonded O1 versus all those that never transferred. Since all of the PTs occurred with the proton in the D1A1 state, which has the strongest H-bond, it can be expected that the proton will remain in a H-bonded state for a longer period of time. That is, the angular displacement of the D1A1 is smaller than the other ranks (figure 10b) and reaching this rank from the other ranks would imply a longer time as a H-bonded state. Overall, this longer H-bonded lifetime for protons that transfer is important in subsequent discussions of the lifetime of the H-bond in the structural diffusion H_3O^+ and OH^- ions.

The major point of these proton transfers is that the large majority involved femtosecond autoionizations of water molecules, creating the H_3O^+ and OH^- ions that returned to their initial neutral water molecule states, consistent with ab-initio calculations, with only a few short loops that returned to the initially-formed OH^- ion to reinstate the neutral water molecules. These rattling autoionizations occurred in protons with long H-bond lifetimes in comparison to the system average. The relevance of such results will be important in long-range proton diffusion, as in the structural diffusion of the H_3O^+ ion and the role of interfaces on such behavior and will be presented in the future.

Conclusion

The structure and lifetimes of hydrogen bonds and auto dissociation via proton transfer in water were studied using the topological definition of the hydrogen bond with a dissociative, all-atom

potential. This potential has previously been shown to reproduce many of the structural and dynamic properties of water and allows for proton transfer in a Grotthuss mechanism involving Eigen-Zundel-Eigen configurations similar to ab-initio calculations, with an activation barrier also similar to ab-initio calculations. The results here show that the behavior of the hydrogen bond is similar to previous experimental and ab-initio data, but with the advantage of using a dissociative potential that allows for proton transfer concurrent with structural variations in large scale simulations. The simulations show that the lifetime of the H-bond related to proton transfer in autoionization of the water molecule is quite distinct from overall H-bond lifetimes.

The simulations using this potential reproduce much of what is known about the structure of H-bonds in water. The OOH angles and the concentration of H-bond distances (r_2 , here) less than 2.4 Å are similar to NMR data. The lifetime of the H-bond, 2.1 ps, is consistent with experimental data, with short time librations on the order of femtoseconds. The angular correlation functions show the same behavior as previous data, as do the angular displacements. Table 4 and the figure 6 indicate that ~8% of the system have a second shell water entering the first shell, consistent with ab-initio calculations. Thus, the methodology and potential function used here reproduces important feature regarding H-bonds in water.

The system's hydrogen bonds are categorized according to their rank relative to other bonds formed by the donor and acceptor molecules. Results show that these detailed structural ranks correspond to different structures and vibrational frequency ranges. In addition to a picture that some hydrogen bonds sporadically change acceptors with large jumps, the simulations also indicate that hydrogen bonds assume a continuum of structures, ranging from strong linear bonds to bifurcated and dangling bonds, and that these structures readily interconvert in response to local structural fluctuations. In particular, the existence of quasi-stable bifurcated bonds whose orientational decay rate differs from linear bonds by only 7% at long timescales is demonstrated. Unlike previous studies, the simulations demonstrate a modest relationship between long-time orientational decay rate and hydrogen bond strength. In addition, the nature and dynamics of dangling protons enable them to librate over an angular range about three times wider than that of a linear hydrogen bond.

An important contribution of this study that employs the dissociative, all-atom potential is the ability to describe the role of detailed types of hydrogen bonds at the donor water and at the acceptor water that strongly influence structure, vibrational spectra, and auto dissociation via proton transfer. The simulations show short-lived dissociation of water molecules that is similar to ab-initio calculations but also provide details that show that all proton transfers occurred with the proton in the D1A1 state, where the proton is the strongest H-bond to the acceptor water with a concurrently weak

covalent bond to its donor water. Hence, the role of the other H-bonds to the acceptor water and on the donor water play an important part in proton transfer and is consistent with the role of a strong electric field caused by local (first and second shell) waters on initiating dissociation.

Acknowledgement: The authors acknowledge support from the National Science Foundation (NSF) Environmental Chemical Science Program of the Division of Chemistry, grant number 1609044. There are no conflicts to declare.

References

1. M. Eigen, *Angew. Chem. Int. Edn. Engl.*, 1964, 3, 1-19.
2. Z. Luz and S. Meiboom, *J. Am. Chem. Soc.*, 1964, 86, 4768-4769.
3. D. Marx, M. E. Tuckerman, J. Hutter and M. Parrinello, *Nature*, 1999, 397, 601-604.
4. U. W. Schmitt and G. A. Voth, *J Chem Phys*, 1999, 111, 9361-9381.
5. D. Marx, M. E. Tuckerman and M. Parrinello, *J. Phys.: Cond. Matt.*, 2000, 12, A153-A159.
6. S. Walbran and A. A. Kornyshev, *J Chem Phys*, 2001, 114, 10039-10048.
7. A. A. Kornyshev, A. M. Kuznetsov, E. Spohr and J. Ulstrup, *J. Phys. Chem. B*, 2003, 107, 3351-3366.
8. H. Lapid, N. Agmon, M. K. Petersen and G. A. Voth, *J Chem Phys*, 2005, 122, 014506.
9. D. Marx, *ChemPhysChem*, 2006, 7, 1848-1870.
10. O. Markovitch, H. Chen, S. Izvekov, F. Paesani, G. A. Voth and N. Agmon, *J. Phys. Chem. B*, 2008, 112, 9456-9466.
11. K. J. Tielrooij, R. L. A. Timmer, H. J. Bakker and M. Bonn, *Phys. Rev. Lett.*, 2009, 102, 198303.
12. H. Chen, G. A. Voth and N. Agmon, *J. Phys. Chem. B*, 2010, 114, 333-339.
13. D. Marx, A. Chandra and M. E. Tuckerman, *Chem. Rev.*, 2010, 110, 2174-2216.
14. M. E. Tuckerman, A. Chandra and D. Marx, *J Chem Phys*, 2010, 133, 124108.
15. L. Dang, *J Chem Phys*, 2003, 119, 6351-6353.
16. M. Tuckerman, K. Laasonen, M. Sprik and M. Parrinello, *J. Phys. Chem.*, 1995, 99, 5749-5752.
17. M. Tuckerman, K. Laasonen, M. Sprik and M. Parrinello, *J Chem Phys*, 1995, 103, 150-161.
18. R. Vuilleumier and D. Borgis, *J. Phys. Chem. B*, 1998, 102, 4261-4264.
19. R. Vuilleumier and D. Borgis, *J. Chem. Phys.*, 1999, 111, 4251-4266.
20. A. Chandra, M. E. Tuckerman and D. Marx, *Phys. Rev. Lett.*, 2007, 99.
21. J. M. J. Swanson, C. M. Maupin, H. Chen, M. K. Petersen, J. Xu, Y. Wu and G. A. Voth, *J. Phys. Chem. B*, 2007, 111, 4300-4314.
22. A. J. Lee and S. W. Rick, *J Chem Phys*, 2011, 134.
23. W. H. Thompson, *Annu. Rev. Phys. Chem.*, 2011, 62, 599-619.
24. T. Hofer, M. Hitzenberger and B. Randolph, *J. Chem. Theory Comput.*, 2012, 8, 3586-3595.
25. K. Park, W. Lin and F. Paesani, *J. Phys. Chem. B*, 2012, 116, 343-352.
26. R. H. Henchman and S. J. Cockram, *Faraday Discuss.*, 2013, 167, 529.
27. G. K. Lockwood and S. H. Garofalini, *J. Phys. Chem. B*, 2013, 117, 4089-4097.
28. A. Ozkanlar, T. Zhou and A. E. Clark, *J Chem Phys*, 2014, 141, 214107.
29. P. Wernet, D. Nordland, U. Bergmann, M. Cavalleri, M. Odelius, H. Ogasawara, L. A. Naslund, T. K. Hirsch, L. Ojamae, P. Glatzel and L. G. M. Pettersson, *Science*, 2004, 304, 995-999.

30. A. Nilsson, C. Huang and L. G. M. Pettersson, *J. Mol. Liq.*, 2012, 176, 2-16.
31. L. G. M. Pettersson and A. Nilsson, *J. Non-Cryst. Solids*, 2015, 407, 399-417.
32. R. H. Henchman, *J. Phys.: Condens. Matter*, 2016, 28, 384001.
33. Q. Hu, H. Zhao and S. Ouyang, *Phys. Chem. Chem. Phys.*, 2017, 19, 21540-21547.
34. N. Agmon, H. J. Bakker, R. K. Campen, R. H. Henchman, P. Pohl, S. Roke, M. Thämer and A. Hassanali, *Chem. Rev.*, 2016, 116, 7642-7672.
35. C. Huang, K. T. Wikfeldt, T. Tokushima, D. Nordlund, Y. Harada, U. Bergmann, M. Niebuhr, T. M. Weiss, Y. Horikawa and M. Leetmaa, *Proc. Natl. Acad. Sci.*, 2009, 106, 15214-15218.
36. A. Nilsson and L. G. M. Pettersson, *Chem. Phys.*, 2011, 389, 1-34.
37. N. Agmon, *Chem Phys Lett*, 1995, 244, 456-462.
38. S. Woutersen and H. J. Bakker, *Phys. Rev. Lett.*, 2006, 96, 138305.
39. P. L. Geissler, C. Dellago, D. Chandler, J. Hutter and M. Parrinello, *Science*, 2001, 291, 2121-2124.
40. A. Hassanli, M. K. Prakash, H. Eshet and M. Parrinello, *Proc. Natl. Acad. Sci.*, 2011, 108, 20410-20415.
41. P. Ben Ishai, S. R. Tripathi, K. Kawase, A. Puzenko and Y. Feldman, *Phys. Chem. Chem. Phys.*, 2015, 17, 15428-15434.
42. T. D. Kühne and R. Z. Khaliullin, *Nat. Commun.*, 2013, 4, 1450.
43. K. Morokuma, *Acc. Chem. Res.*, 1977, 10, 294-300.
44. H. Umeyama and K. Morokuma, *J. Am. Chem. Soc.*, 1977, 99, 1316-1332.
45. R. H. Henchman and S. J. Irudayam, *J. Phys. Chem. B*, 2010, 114, 16792-16810.
46. R. Kumar, J. R. Schmidt and J. L. Skinner, *J Chem Phys*, 2007, 126, 204107.
47. D. Laage, G. Stirnemann, F. Sterpone and J. T. Hynes, *Acc Chem Res*, 2012, 45, 53-62.
48. D. Laage and J. T. Hynes, *Science*, 2006, 311, 832-835.
49. D. Laage and J. T. Hynes, *J. Phys. Chem. B*, 2008, 112, 14230-14242.
50. D. Laage, G. Stirnemann, F. Sterpone, R. Rey and J. T. Hynes, *Annu. Rev. Phys. Chem.*, 2011, 62, 395-416.
51. H. K. Nienhuys, R. A. van Santen and H. J. Bakker, *J Chem Phys*, 2000, 112, 8487-8494.
52. C. P. Lawrence and J. L. Skinner, *J Chem Phys*, 2003, 118, 264-272.
53. D. Laage and J. T. Hynes, *Chem Phys Lett*, 2006, 433, 80-85.
54. T. S. Mahadevan and S. H. Garofalini, *J. Phys. Chem. B*, 2007, 111, 8919-8927.
55. H. Xu, H. A. Stern and B. J. Berne, *J. Phys. Chem. B*, 2002, 106, 2054-2060.
56. T. S. Mahadevan and S. H. Garofalini, *J. Phys. Chem. C*, 2008, 112, 1507-1515.
57. S. H. Garofalini, T. S. Mahadevan, S. Xu and G. W. Scherer, *ChemPhysChem*, 2008, 9, 1997-2001.
58. S. Xu, G. W. Scherer, T. S. Mahadevan and S. H. Garofalini, *Langmuir*, 2009, 25, 5076-5083.
59. S. Xu, G. C. Simmons, T. S. Mahadevan, G. W. Scherer, S. H. Garofalini and C. Pacheco, *Langmuir*, 2009, 25, 5084-5090.
60. G. K. Lockwood and S. H. Garofalini, *J. Phys. Chem. C*, 2014, 118, 29750-29759.
61. N. Agmon, *J. Phys. Chem. A*, 2005, 109, 13-35.
62. M. E. Tuckerman, D. Marx and M. Parrinello, *Nature*, 2002, 417, 925-929.
63. D. Wolf, P. Keblinski, S. R. Phillpot and J. Eggebrecht, *J Chem Phys*, 1999, 110, 8254-8282.
64. R. A. DiStasio, B. Santra, Z. Li, X. Wu and R. Car, *J Chem Phys*, 2014, 141.
65. K. Modig, B. G. Pfrommer and B. Halle, *Phys. Rev. Lett.*, 2003, 90.
66. M. Hakala, K. Nygård, S. Manninen, S. Huotari, T. Buslaps, A. Nilsson, L. G. M. Pettersson and K. Hämäläinen, *J Chem Phys*, 2006, 125, 084504.
67. S. Woutersen, U. Emmerichs and H. J. Bakker, *Science*, 1997, 278, 658-660.
68. B. Reischl, J. Kofinger and C. Dellago, *Mol. Phys.*, 2009, 107, 495-502.

TABLE CAPTIONS:

Table 1: Table 1. 2-body and 3-body terms in the interatomic potential.

Table 2: Probability distribution of molecular coordination states. The type of species, determined by an oxygen's number of covalent protons and number of donated hydrogen bonds, is shown in the left-hand column. The middle column specifies the number of accepted hydrogen bonds, and the right-hand column is the fraction of the system's molecules which are in the specified coordination state.

Table 3: Probability that a proton forms a bond of a given rank, or that it is dangling.

Table 4: Probability that a hydrogen's O_3 is bonded to O_1 , O_2 , neither, or both, for each bond rank. If O_3 is bonded to both O_1 and O_2 , then O_1 , O_2 , and O_3 form a three-member cycle.

Table 5: Decay constants of first-order and second-order correlation functions at long timescales, calculated between $t=3\text{ps}$ and $t=4\text{ps}$. A modest but non-negligible rank-dependence is observed. The libration cone half-angle was estimated from the data shown in figure 10b

Table 6: Characteristics of linear, bifurcated, and dangling bonds. While hydrogen bonds exhibit a wide continuum of structures and lifetimes, the observed trends are summarized by these categories.

FIGURE CAPTIONS:

Figure 1. (a) Overall O_2 - O_1 -H bond angle for the full system. (b) Hydrogen bond distance (r_2) for all HBs in the water. Inset in 1b shows the H_i and O labels and r_1 , r_2 , and r_3 distances.

Figure 2. The HO pair distribution functions for each labeled rank in the system showing differences in the hydrogen bond distances (r_2) for the ranks and similar distances for the r_3 and r_4 distances (distance between a proton and its 3rd and 4th O neighbors). Inset shows the H_i and O labels and r_1 , r_2 , and r_3 distances.

Figure 3. (a) r_1 distance (proton distance to its covalently bonded O) showing longest OH bond for the proton in the D1A1 state and shortest in the Dangling state; (b) r_2 distance, which is the hydrogen bond distance between a proton and its acceptor oxygen showing the shortest HB distance for those protons that in (a) had the longest covalent bond length; (c) r_3 distance showing protons with A1 rank have narrowest distribution of distances to 3rd O; (d) r_4 distance just slightly longer than r_3 distances. Inset in a-c show the O labels and the r_1 , r_2 , and r_3 distances.

Figure 4. O_1 - O_2 pair distribution functions showing longer distances with higher rank protons. Short distance tail on D1A1 presages more likely proton transfer for these protons.

Figure 5. (a) O2-O1-H bond angles showing most protons have bond angles less than $\sim 30^\circ$, fitting one common geometrical criterion for the hydrogen bond; (b) O3-O1-H bond angle with dual peaks determined by the relationship between O3 and O1 or O3 and O2, as shown in (c) which shows the O3-O1-H angle for O3 bonded to O1 or O2 or both or neither and a lower peak for O3 H-bonded to O2 than for O3 H-bonded to O1.

Figure 6. The δ distributions showing the difference in r_3-r_2 distances and the linear (large δ distributions) versus bifurcated bonds (low δ distributions). While qualitative, one could arbitrarily separate the types of bonds using a cutoff of 0.9\AA , with δ for bifurcated bonds $< 0.9\text{\AA}$ and for linear bonds $> 0.9\text{\AA}$.

Figure 7. The high frequency peak as a function of bond rank consistent with the r_1 distances and lower OH vibrational frequency for the longer r_1 in D1A1 to the higher frequencies for the shorter r_1 's.

Figure 8. (a) The overall H-bond continuous lifetime correlation function showing an exponential decay at longer times, with a time constant of 2.1 ps; (b) the hydrogen bond correlation functions for the differently ranked protons showing much more rapid decay of the bond for specific configurations in comparison to the overall H-bond results of (a), indicating the multiple short-lived localized states of the H-bond while maintaining a longer-lived H-bond; (c) short-time femtosecond behavior of ranks.

Figure 9: (a) First-order and (b) second-order angular correlation functions according to proton rank. The rapid sub-picosecond decay, as commonly acknowledged, is due to librational rotation contained within a cone; the bumps seen at 0.05ps to 0.1ps result from protons reaching the end of their range and rebounding toward their initial orientations. Beyond 1.5ps, all angular correlation functions decay monoexponentially. The long-timescale decay rates (shown in table 5) depend modestly on rank, and therefore, bond strength.

Figure 10: (a) Distributions of instantaneous angular velocities of protons about their covalent oxygens, by rank. A slight rank-dependence exists, with a difference between bonding and dangling protons, leading to the conclusion that librational rotation rates are weakly dependent of hydrogen bond strength. (b) Mean angular displacements by rank; the dashed line represents the angular displacement of a proton rotating freely at the modal angular velocity. The intersection of this line with each angular displacement function provides an estimate of the rank's mean libration cone half-angle; the values obtained are shown in Table 5.

Figure 11. (a) Median r_1 covalent bond lengths for all D1A1 (dotted line) and all D1A1 that showed auto dissociation via proton transfer (PT). (b) Median r_1 , r_2 (H-bond length) and O1-O2

distance for all D1A1 (dotted lines) and for all D1A1 that showed PT (the latter as a function of time prior to the PT event, which occurred at time=0).

Figure 12. The lifetimes of four autoionization events and their associated hydrogen bonds. Red line is the time of the H-bond at the site and the blue line is the time at which the proton exists on the acceptor O, returning to the original donor O at the end of the blue line. See text for details.

Figure 13. The continuous H-bond lifetime autocorrelation function for all protons that transferred from their original covalently bonded O1 versus all those that never transferred.

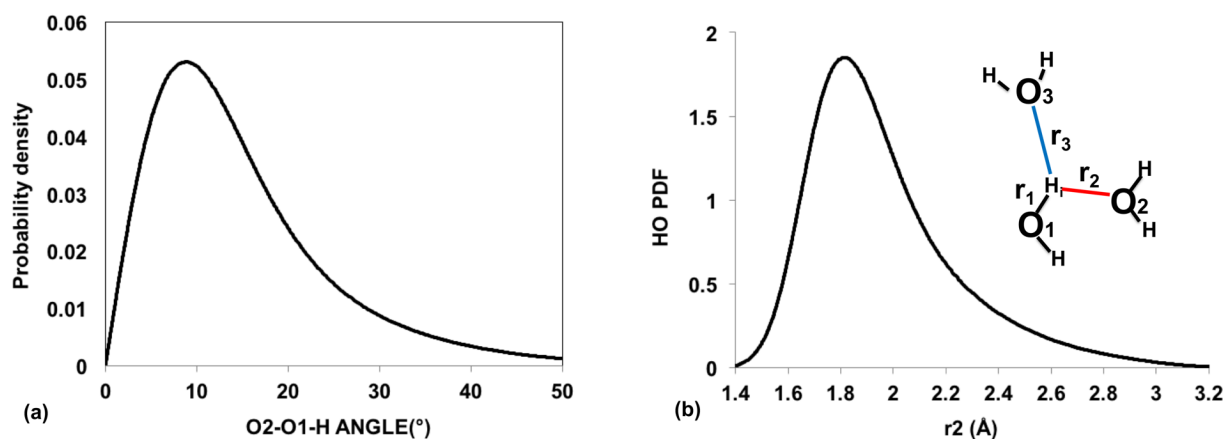


Figure 1. (a) Overall O2-O1-H bond angle for the full system. (b) Hydrogen bond distance (r_2) for all HBs in the water. Inset in 1b shows the H_i and O labels and r_1 , r_2 , and r_3 distances.

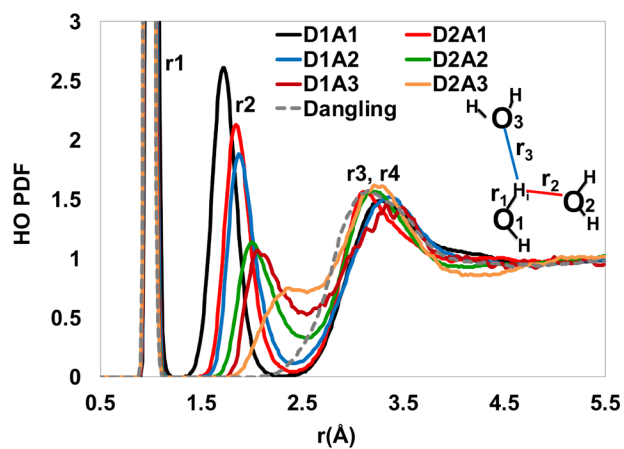


Figure 2. The HO pair distribution functions for each labeled rank in the system showing differences in the hydrogen bond distances (r_2) for the ranks and similar distances for the r_3 and r_4 distances (distance between a proton and its 3rd and 4th O neighbors). Inset shows the H_i and O labels and r_1 , r_2 , and r_3 distances.

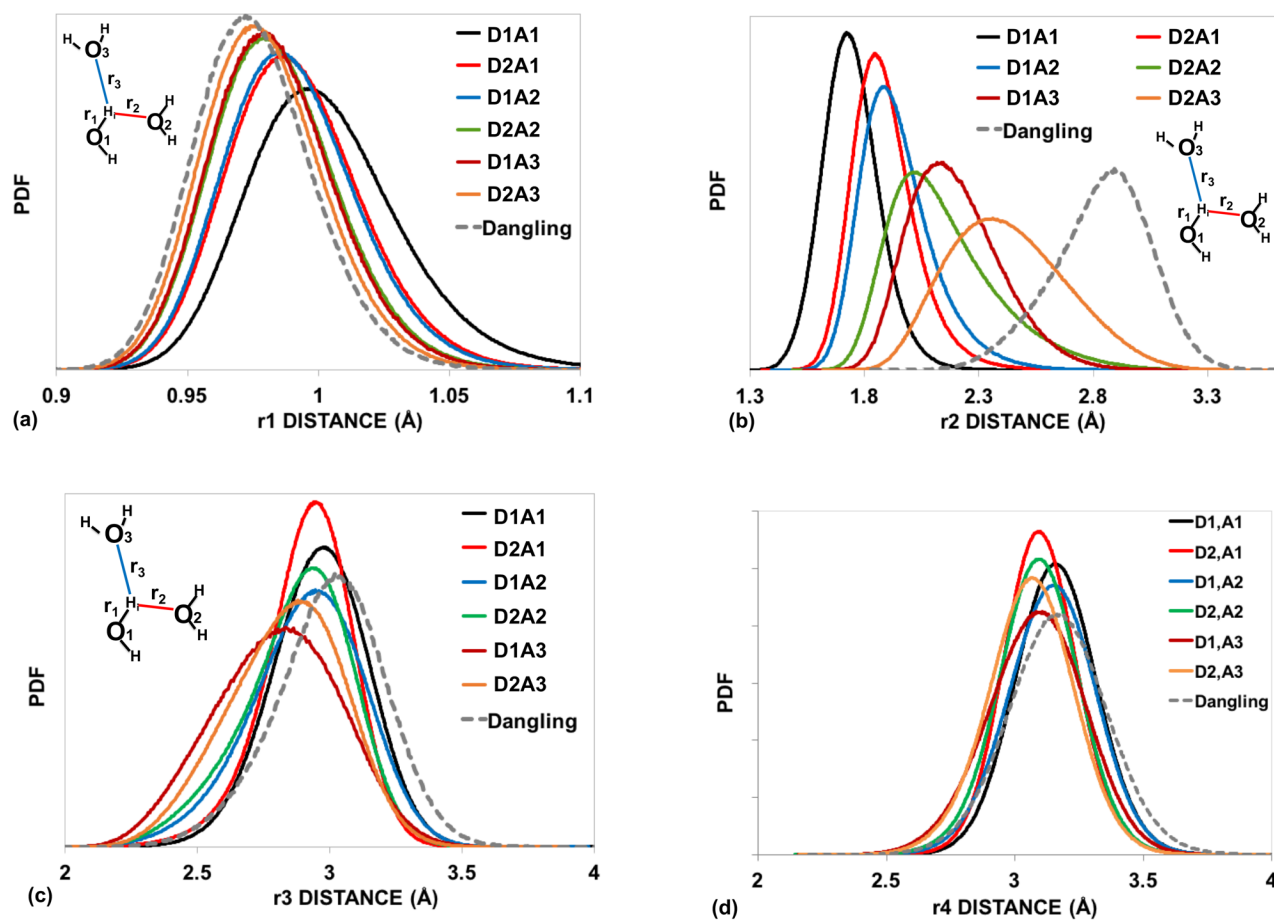


Figure 3. (a) r_1 distance (proton distance to its covalently bonded O) showing longest OH bond for the proton in the D1A1 state and shortest in the Dangling state; (b) r_2 distance, which is the hydrogen bond distance between a proton and its acceptor oxygen showing the shortest HB distance for those protons that in (a) had the longest covalent bond length; (c) r_3 distance showing protons with A1 rank have narrowest distribution of distances to 3rd O; (d) r_4 distance just slightly longer than r_3 distances. Insets show the H_i and O labels and r_1 , r_2 , and r_3 distances.

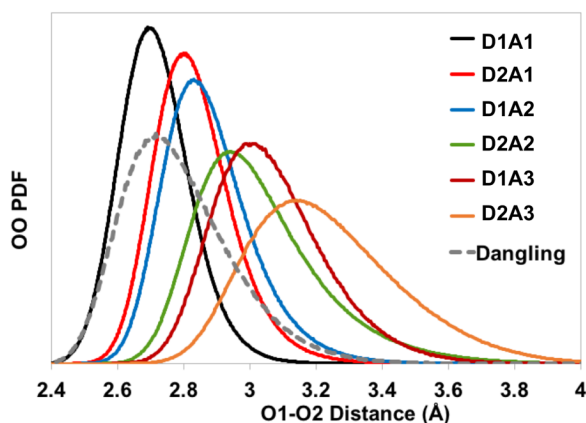


Figure 4. O1-O2 pair distribution functions showing longer distances with higher rank protons. Short distance tail on D1A1 presages more likely proton transfer for these protons.

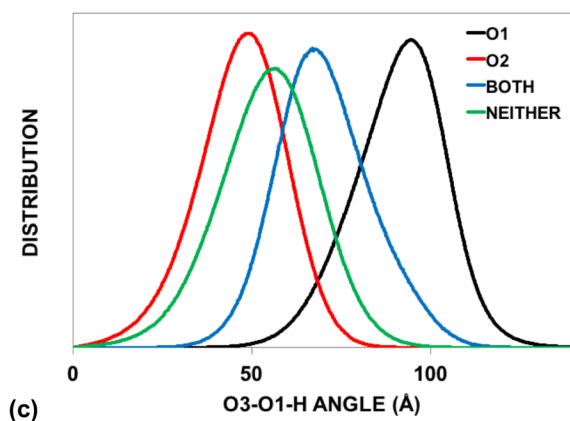
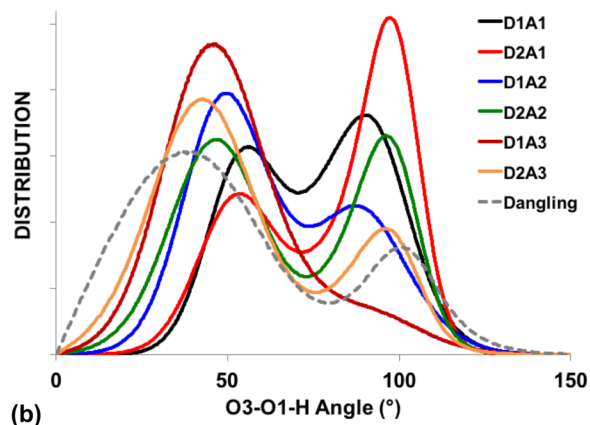
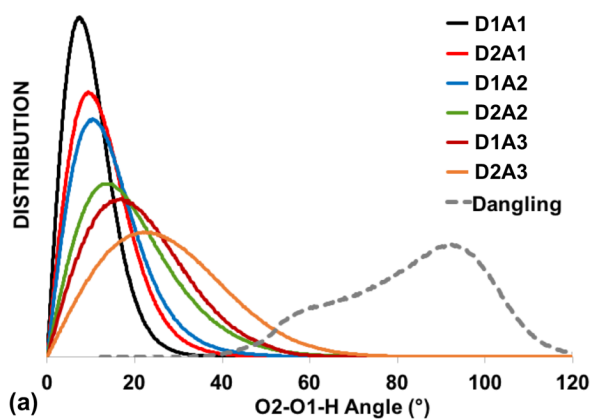


Figure 5. (a) O2-O1-H bond angles showing most protons have bond angles less than $\sim 30^\circ$, fitting one common geometrical criterion for the hydrogen bond; (b) O3-O1-H bond angle with dual peaks determined by the relationship between O3 and O1 or O3 and O2, as shown in (c) which shows the O3-O1-H angle for O3 bonded to O1 or O2 or both or neither and a lower peak for O3 H-bonded to O2 than for O3 H-bonded to O1.

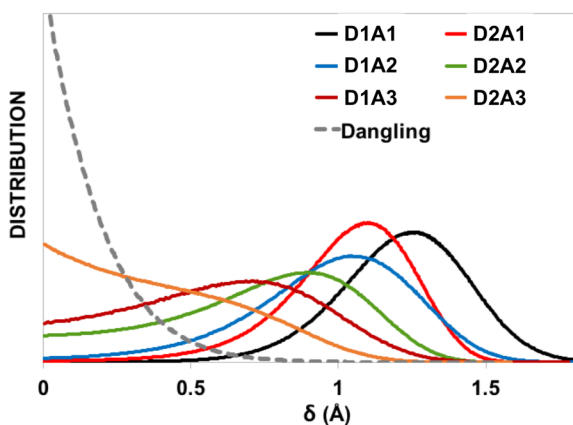


Figure 6. The δ distributions showing the difference in r_3 - r_2 distances and the linear (large δ distributions) versus bifurcated bonds (low δ distributions). While qualitative, one could arbitrarily separate the types of bonds using a cutoff of 0.9\AA , with δ for bifurcated bonds $< 0.9\text{\AA}$ and for linear bonds $> 0.9\text{\AA}$.

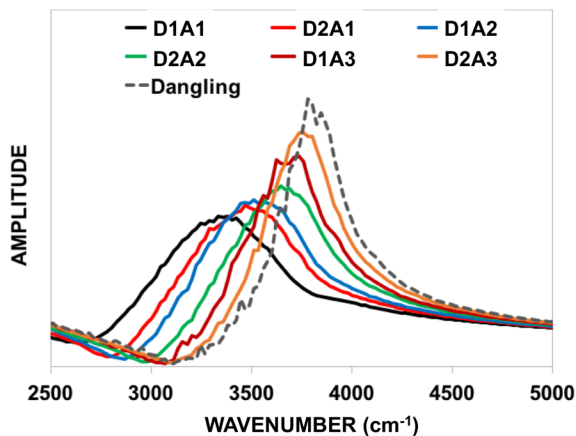


Figure 7. The high frequency peak as a function of bond rank consistent with the r_1 distances and lower OH vibrational frequency for the longer r_1 in D1A1 to the higher frequencies for the shorter r_1 's.

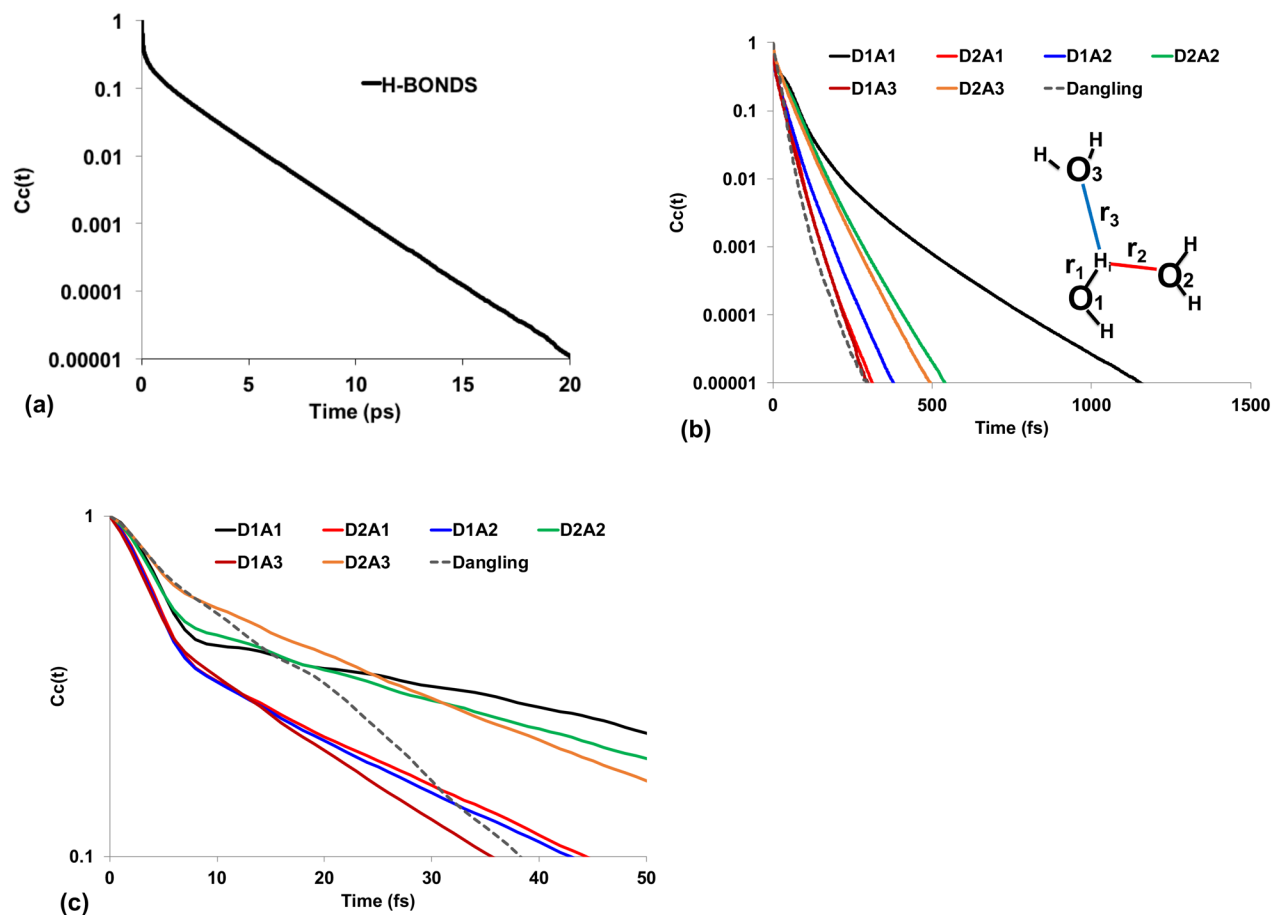


Figure 8. (a) The overall H-bond continuous lifetime correlation function showing an exponential decay at longer times, with a time constant of 2.1 ps; (b) the hydrogen bond correlation functions for the differently ranked protons showing much more rapid decay of the bond for specific configurations in comparison to the overall H-bond results of (a), indicating the multiple short-lived localized states of the H-bond while maintaining a longer-lived H-bond; (c) short-time femtosecond behavior of ranks. Inset in (b) shows the H_i and O labels and r_1 , r_2 , and r_3 distances.

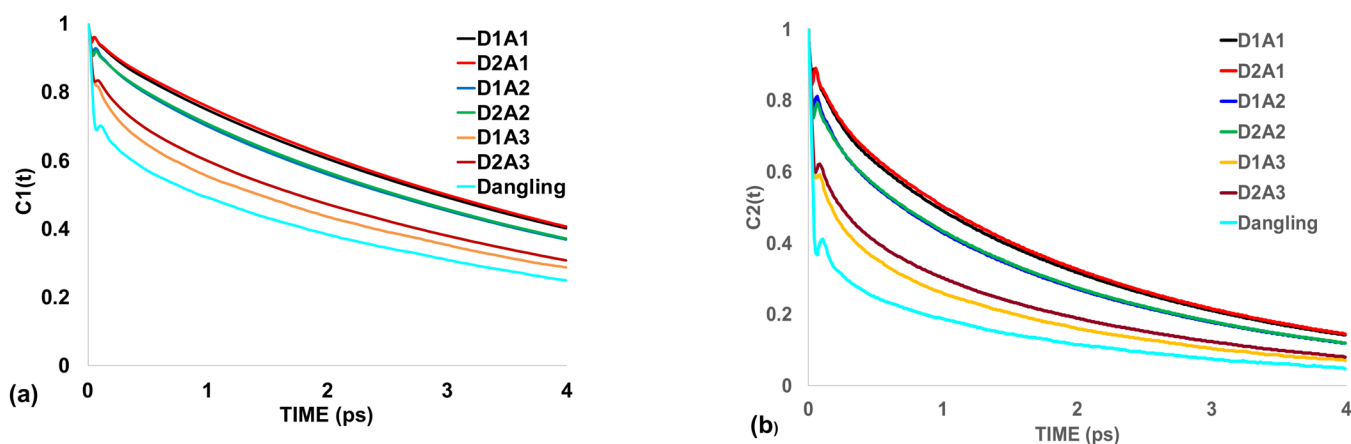


Figure 9: (a) First-order and (b) second-order angular correlation functions according to proton rank. The rapid sub-picosecond decay, as commonly acknowledged, is due to librational rotation contained within a cone; the bumps seen at .05ps to .1ps result from protons reaching the end of their range and rebounding toward their initial orientations. Beyond 1.5ps, all angular correlation functions decay monoexponentially. The long-timescale decay rates (shown in table 5) depend modestly on rank, and therefore, bond strength.

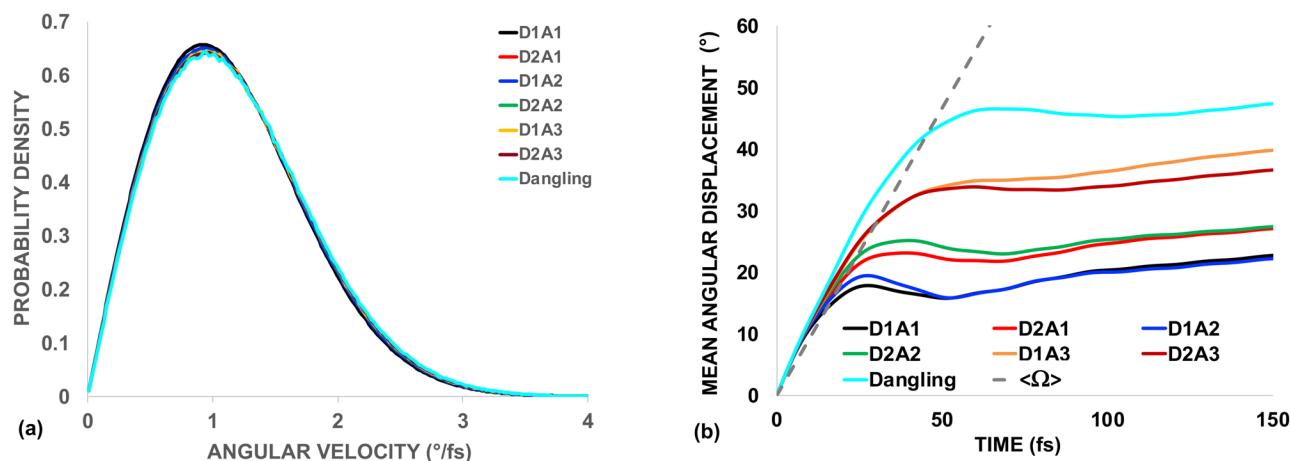


Figure 10: (a) Distributions of instantaneous angular velocities of protons about their covalent oxygens, by rank. A slight rank-dependence exists, with a difference between bonding and dangling protons, leading to the conclusion that librational rotation rates are weakly dependent of hydrogen bond strength. (b) Mean angular displacements by rank; the dashed line represents the angular displacement of a proton rotating freely at the modal angular velocity. The intersection of this line with

each angular displacement function provides an estimate of the rank's mean libration cone half-angle; the values obtained are shown in Table 5.

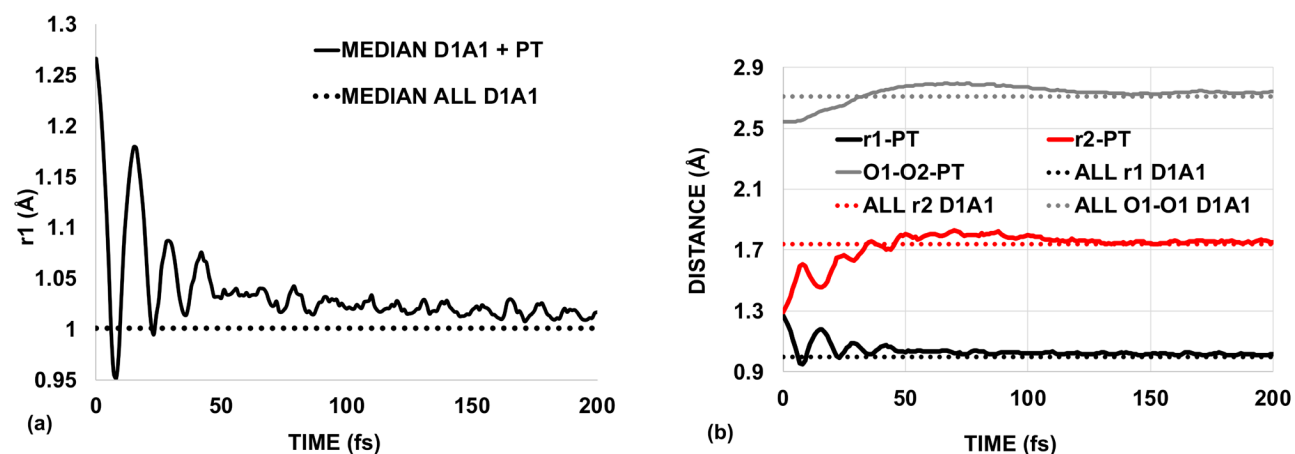


Figure 11. (a) Median r1 covalent bond length for all D1A1 (dotted line) and all D1A1 that showed auto dissociation via proton transfer, PT (the latter as a function of time prior to the PT event, which occurred at time=0). (b) Median r1, r2 (H-bond length) and O1-O2 distance for all D1A1 (dotted lines) and for all D1A1 that showed PT (the latter as a function of time prior to the PT event, which occurred at time=0).

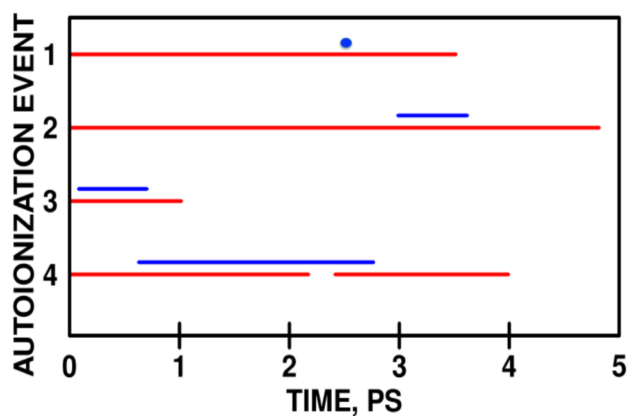


Figure 12. The lifetimes of four autoionization events and their associated hydrogen bonds. Red line is the time of the H-bond at the site and the blue line is the time at which the proton exists on the acceptor O, returning to the original donor O at the end of the blue line. See text for details.

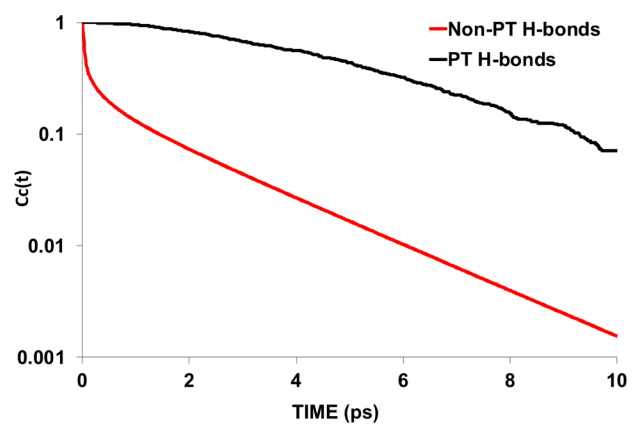


Figure 13. The continuous H-bond lifetime autocorrelation function for all protons that transferred from their original covalently bonded O1 versus all those that never transferred.